Studies on Defect Detection and Thermal Influence in SiC Substrates Using an IR Thermal Imaging Camera

Passapong Wutimakun*, Karuan Chaivanich, Theerachol Mahawan
Thongkam Chumpol, Winat Intarasuwan, and Chumpol Buteprongjit
Chulachomklao Royal Military Academy

Abstract

A long-wavelength infrared thermal imaging camera was applied to visually evaluate the thermal influence of defects in SiC substrates. Defects in substrates were rapidly and effectively detected by IR camera observation, and the dependence of the temperature on the defect size could be observed precisely. IR camera was applied to show clearly the change in heat propagation in areas of defects in SiC substrates by observation of temperature distribution images in real time. Consequently, the IR camera can be considered as an effective technique for evaluating the thermal influence of defects.

Keywords : SiC, IR camera, defect, heat propagation, temperature distribution image.

1. Introduction

Silicon carbide (SiC) is a promising material for the next generation of semiconductors because of its ability to operate at high temperature, high frequency and high power. [1] SiC is expected to serve as a substrate material for high-frequency devices based on GaN. [2, 3] Recently, very low-defect density SiC substrates have been developed to meet these requirements. [4, 5] However, characterization of the thermal influence of defects in these substrates is still important before such substrates can actually be applied in high frequency devices.

To detect the defects that present in SiC substrate, scanning laser microscopes [6, 7] light-scattering tomography [8, 9], polarized optical microscope [10, 11], X-ray topography [12, 13] and photoluminescence mapping [14] have been used. Although these methods can effectively detect defects, they cannot visually show the thermal influence of defects in SiC substrate for the same time. Therefore, in this study, a long-wavelength infrared thermal imaging camera (IR camera) that is considered as effective technique for evaluating the defects and the thermal influence of defects in SiC single crystal was proposed.

Attempts to measure the thermal diffusivity of solids using IR camera technology have recently been reported, [16, 17] and such a camera has been used to investigate the operating characteristics of a heat sink structure. [18] IR cameras are widely applied to determine the thermal properties of materials. In this study, IR camera evaluation technology was applied to perform a non-destructive defect detection in SiC crystals and to examine the thermal influence of defects.

* Department of Industrial Engineering, Chulachomklao Royal Military Academy

2. Experiments

2.1. Sample Fabrications

The samples used in this study were commercial 6H-SiC single crystals grown using the conventional sublimation method; the seed temperature and the pressure were kept at 2100–2300 °C and 1.3 kPa (10 Torr) to 2.6 kPa (20 Torr), respectively, during crystal growth. Samples were cut with a size of $5\times25\times1$ mm^3 perpendicular to the [0001] axis from two different 6H-SiC wafers. In this experiment, sample A was cut from 6H-SiC wafer that had the quality of crystal better than sample B. The sample surfaces were mirror polished.

2.2. Methods

Firstly, we observed and classified the defects in each sample using an IR camera (NEC Avio, TH 9100 MR) as shown in Fig.1. An IR camera detects and visualizes infrared light radiated from materials. If a substrate contains defects or distortions, the thermal properties of these areas will be changed compared with the periphery. Therefore, these areas show a different temperature. Using the intensity of infrared radiation, one can detect defects and distortions in a substrate conveniently and accurately. The intensity of infrared radiation can be described by Stefan–Boltzmann law as follows:

$$E=\sigma T^4 \tag{1}$$

Where E is the intensity of infrared radiation per unit area (W/m2), σ is the Stefan–Boltzmann constant (equal to 5.6704×10-8 W/m2K4), and T is the absolute temperature (K) [15]. A long-wavelength IR camera was used with an uncooled 2D microbolometer array as a detector and measurement range of -20 to 250 °C. The thermal sensitivity and spectral range of this camera were 0.02 K at 303 K and 8–14 μm, respectively. A 25 μm close-up lens (WI-259D) was used, where the minimum detection range was 25×25 μm. The samples were heated by an electric heating plate (AS ONE, ND-1) and observed on a flat copper plate. To decrease the background noise, the sample and camera were enclosed in a shielding box. The resulting images were cleaned up by image-processing software (NEC Avio, NS 9200). The differences in temperature between the defect areas and the periphery could be detected directly, as the IR emissivity of the copper plate was much lower than that of the SiC.

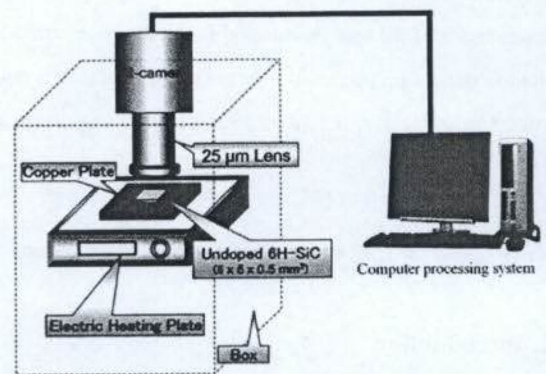

Fig.1. Schematic diagram of the IR camera observations.

The use of an IR camera is a rapid and effective technique for the detection of defects, but it cannot observe the shapes of defects in detail. Therefore, we zoomed in on the defect areas in the IR camera images to estimate the defect shapes using scanning laser microscopy (SLM) [6, 7] and three-dimensional light-scattering tomography (3D-LST), [6, 9] as described later.

Finally, an experimental study of heat propagation in the samples was performed. The conditions were similar to those in the defect detection studies. For the heating system, a deposited one-dimensional heater was used, where a width of about 0.5 mm of Ni was

deposited at one end of each sample. The Ni-deposited samples were heat-treated for 3 min at 1050 °C in an Ar atmosphere. A DC power supply (Kenwood, PA18-3A) was used, to obtain a clear image. The power supply was set to 6.00 V and 0.10 A for observing the behavior of heat propagation in the samples. The entire samples were observed for 4 s, and 20 observations of the temperature distribution image were made at 0.2 s intervals. In addition, the thermal diffusivity of the samples was also evaluated by a differential photopyroelectric (PPE) method [7] compared to the results of IR camera.

3. Results and discussion

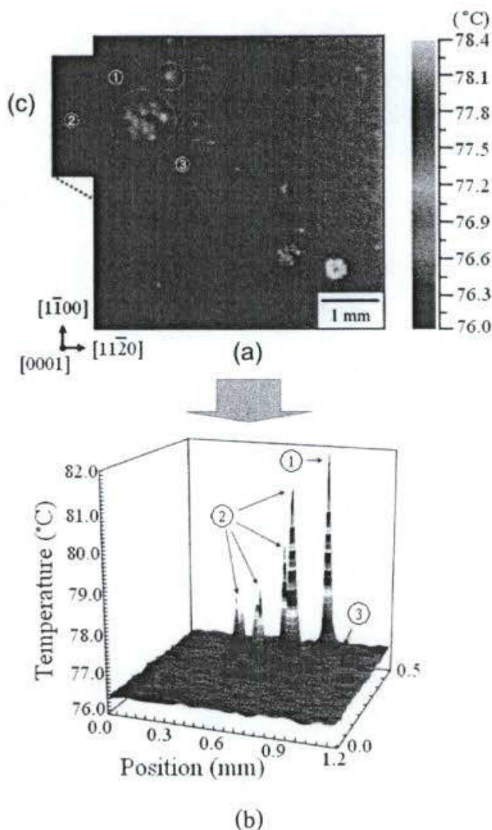

Fig.2. Temperature distribution image of sample B obtained with IR camera

Sample A shows an almost uniform color, which means a uniform temperature. However, sample B, shown in the two-dimensional IR camera image of Fig. 2(a), shows various colors, which means a nonuniform temperature. The white points in the image of sample B are defects, and the high temperatures around the defects are considered to be a result of the thermal influence of the defects.

We could confirm that the defects in sample B were more numerous than those in sample A. To further investigate the temperature distribution around the defects detected in the IR camera images, the temperature profile of the surface of the samples was analyzed by the use of image-processing software. By this method, we could study the temperature around each defect in detail. The temperature resolution and the detection range were set to 0.1 K and 25×25 μm2, respectively. The images of samples B was analyzed as shown in Figs. 2(b). The temperature distributions in the 3D image of sample B in the defect areas shown as points 1, 2, and 3 in Fig. 2(b) were clearly different from that in the normal area, and each defect area also had a temperature distribution that was different from that of the others in terms of scale and maximum temperature. These differences in the temperature distribution in sample B were caused by differences in defect size. [16]

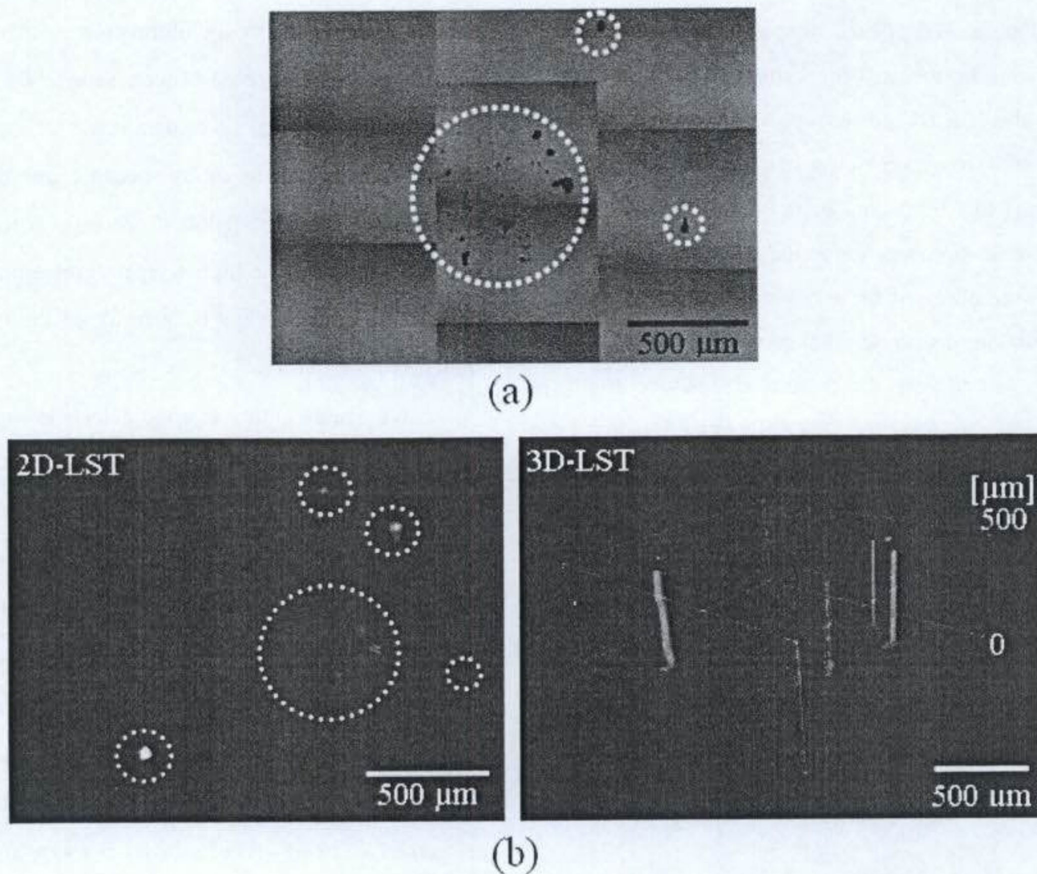

Fig. 3. Observation of the shape of defects on the surface using SLM and LST in the IR camera image of Fig. 2(c). (a) SLM image; (b) 2D- and 3D-LST images.

Next, we zoomed in on the defect area in sample B shown in Fig. 2(c) to observe the shapes of the defects on the surface using SLM and LST. The results are shown in Figs. 3(a) and (b), respectively. The irregular black spots in Fig. 3(a) were considered to be micropipes and clusters of impurities. The size of the defects was calculated from the SLM image (600×800 μm2) and was found to be 5-10 μm. We also applied 3D-LST to observe the depth distribution of the defects. The results showed that the defects observed in sample B were not only located on the substrate surface but also continued into the substrate, as shown in Fig. 3(b).

The large point-like and rod-like scattering patterns were considered to be the outlines of defects decorated by impurity precipitates and of hollow defects such as micropipes, respectively. [19] The results confirmed that the presence of defects can affect the nonuniformity of the temperature in SiC. Since the thermal conductivity in a defect area is smaller than that in the surrounding area, the amount of infrared radiation in the IR camera observation is different, and this shows as a nonuniform temperature distribution in the IR camera image. [16]

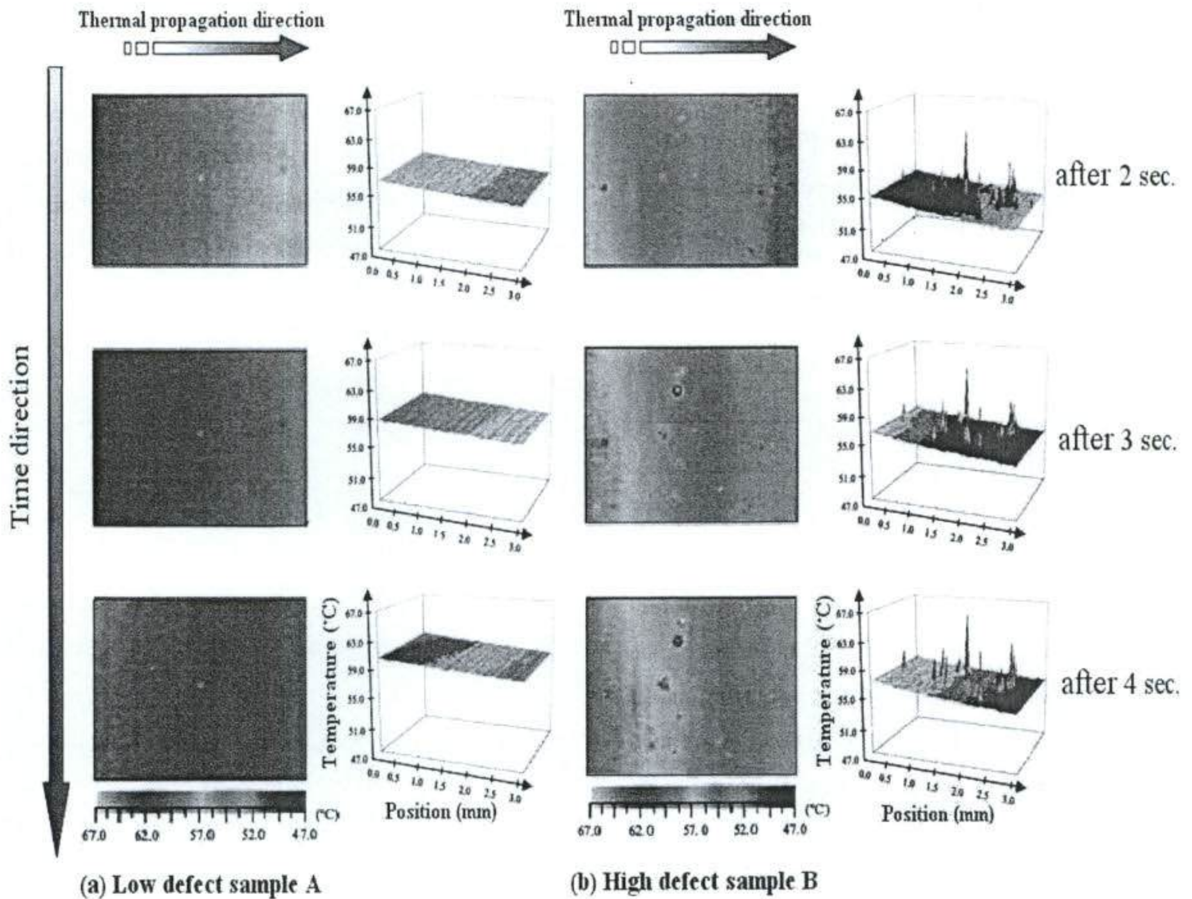

Fig.4. the Ni electrode was heated at the end of each sample for 4 s to visually observe heat propagation in the samples with the IR camera in real time.

Finally, the Ni electrode was heated at the end of each sample for 4 s to visually observe heat propagation in the samples with the IR camera in real time. 2D and 3D IR camera images of each sample are shown in Fig. 4. In the low-defect sample A, as shown in Fig. 4(a), the temperature range was 56–60 °C after 2 s of heating, 60–63 °C after 3 s, and 63–67 °C after 4 s. The thermal behavior in the 3D images showed a smooth propagation. In contrast, the temperature range in sample B was 51–56 °C after 2 s, 53–54 °C after 3 s, and 54–58 °C after 4 s. At the same heating times, the heat propagation behavior of sample B, as shown in Fig. 4(b), was rather poor in comparison with that of sample A. Furthermore, 3D images of sample B showed that the variable scatter of the heat propagation was caused by a change in the thermal conductivity around the defect areas. [20, 21] The thermal diffusivity of the samples was also evaluated by a differential photopyroelectric (PPE) method [7] to support the results of the heat propagation studies as shown in table 1. These values corresponded with the results obtained from IR camera observation. As the above results indicate, the IR

camera observation is an effective method to examine the thermal property in 6H-SiC.

Table 1 Comparison of thermal diffusivity of the samples between the PPE method and the IR camera observation.

Sample	Thermal diffusivity (cm^2/s)	
	IR camera	PPE method
Sample A	1.62	1.61
Sample B	1.25	1.25

4. Conclusion

In this study, we have shown that defect detection in semi-insulating 6H-SiC substrates can be performed with a wide viewing range using an IR camera, and it is expected that all defects in a 4-inch SiC wafer could be detected within a few minutes. Furthermore, IR camera observation provides a nondestructive, rapid and effective method for defect detection in SiC substrates. In particular, we have successfully used an IR camera to visually show the changes in heat propagation due to defects in semiinsulating 6H-SiC substrates, by recording temperature distribution images in real time. The results in this study prove that defects in SiC substrates have a harmful influence on the thermal properties of the substrate. This is important information for the development of the semi-insulating 6H-SiC substrates that are expected to serve as a substrate material for GaN high-frequency devices.

Acknowledgments

This research was financially supported by Prof. Dr. Jun Morimoto (National Defense Academy, Japan)

References

1) H. Matsunami: Jpn. J. Appl. Phys. **43** (2004) 6835.
2) V. Kumar, D. H. Kim, A. Basu and I. Adesida: IEEE Electron Device Lett. **29** (2008)18.
3) A. L. Corrion, C. Poblenz, F. Wu and J. S. Speck: J. Appl. Phys. **103** (2008) 093529.
4) C. Longeaud, J. P. Kleider, P. Kaminski, R. Kozlowski and M. Miczuga: J. Phys.: Condens. Matter **21** (2009) 045801.
5) L. Ning, Z. Feng, Y. Wang, K. Zhang, Z. Feng and X. Xu: J. Mater. Sci. Technol. **25** (2009) 102.
6) P. Wutimakun, C. Buteprongjit and J. Morimoto: J. Cryst. Growth **311** (2009) 3781.
7) P. Wutimakun, H. Miyazaki, Y. Okamoto, J. Morimoto, T. Hayashi and H. Shiomi: Mater. Sci. Forum **600** (2009) 521.
8) L. Taijing, K. Toyoda, N. Nango and T. Ogawa: J. Cryst. Growth **114** (1991) 64.
9) P. Wutimakun, T. Mori, H. Miyazaki, Y. Okamoto and J. Morimoto: Jpn. J. Appl. Phys. **47** (2008) 5576.
10) X. Ma and T. Sudarshan: J. Electro. Mater. **33** (2004) 450
11) P. Wutimakun and J. Morimoto: to be published in Jpn. J. Appl. Phys.
12) X. Ma, M. Dudley, W. Vetter and T. Sudarshan: Jpn. J. Appl. Phys. **42** (2003) L1077.
13) H. Yamaguchi and H. Matsuhata: J. Electron. Mater. **39** (2010) 715.
14) G. Fenga, J. Suda and T. Kimotoa: Physics B **404** (2009) 4745.
15) I.Montvay and E. Pietarinen: Physics Lett. B **110** (1982) 148.
16) K. Lee, H. Miyazaki, Y. Okamoto and J. Morimoto, Mater. Sci. Forum **645** (2010) 559.

17) K. Lee, H. Miyazaki, Y. Okamoto, J. Morimoto and K. Toda: to be published in Jpn. J. Appl. Phys.

18) R. Boukhanouf , A. Haddad, M. T. North and C. Buffone, Appl. Therm. Eng. **26** (2006) 2148.

19) B.G. Vainer, G.N. Kamaev and G.L. Kurishev, J. Cryst. Growth **210** (2000) 351.

20) J. Morikawa and T. Hashimoto, 15th Symposium on Thermophysical Properties, 2003, p. 578.

21) S. Wu, P. Geiser, J. Jun, J. Karpinski and R. Sobolewski : Phys. Rev. B **76** (2007) 085210.